Appl Phys B (2011) 103: 75–82
DOI 10.1007/s00340-010-4288-z

Applied Physics B
Lasers and Optics

Dual-wavelength oscillation at 1064 and 1342 nm in a passively Q-switched Nd:YVO_4 laser with V^{3+}:YAG as saturable absorber

J.-L. Xu · H.-T. Huang · J.-L. He · J.-F. Yang · B.-T. Zhang · X.-Q. Yang · F.-Q. Liu

Received: 25 May 2010 / Revised version: 3 September 2010 / Published online: 6 November 2010
© Springer-Verlag 2010

Abstract The efficient dual-wavelength oscillation at 1064 and 1342 nm in the passively Q-switched laser based on Nd:YVO_4/V^{3+}:YAG is successfully obtained, as demonstrated in this paper. A total average output power of 2.2 W is obtained with 1.3 W for 1064 nm and 0.9 W for 1342 nm under the incident pump power of 7.7 W, corresponding to a total optical-optical conversion efficiency of 28.2%. The pulse widths are 58 and 54 ns for 1064 and 1342 nm, respectively, with the repetition rate of 89 kHz. Moreover, a rate equation model considering the Gaussian spatial distributions of the intracavity photon density and the initial population-inversion density is presented to characterize the dual-wavelength passive Q-switching operation.

1 Introduction

Multi-wavelength lasing operation of Nd^{3+} ion-doped host materials has attracted great interest for the wide application in optical communication, medical instrumentation, nonlinear optical frequency conversion, and so on. The allowed quasi-three-level transition from $^4F_{3/2}$-$^4I_{9/2}$, and four-level transition from $^4F_{3/2}$-$^4I_{11/2}$ and $^4F_{3/2}$-$^4I_{13/2}$ of Nd^{3+} ion-doped host materials, corresponding to the respective wavelengths of 0.94, 1.06 and 1.34 μm, show promise for simultaneous multi-wavelength lasing. Continuous-wave simultaneous dual-wavelength emissions at 1.0 μm and either of 0.9 and 1.3 μm have been actively reported [1–5]. Moreover, the Q-switched simultaneous dual-wavelength operation at 1.0 and 1.3 μm has been realized in Nd:YAG laser by using an acousto-optic Q-switcher [6]. The frequency mixing of the 1.0 and 1.3 μm pulsed lasers overlapping in the non-linear crystals is a practical approach to generating a yellow-orange laser, which is of great importance in dermatology and ophthalmology due to the high absorption in hemoglobin.

The nanosecond laser pulses of 0.9, 1.0 or 1.3 μm with high energy can be obtained from the lasers Q-switched by the saturable absorbers such as Cr^{4+}:YAG, V^{3+}:YAG, Co^{2+}:LGO, and so on [7–10]. A simultaneous dual-wavelength Q-switched Nd:YAG laser at 0.9 and 1.0 μm was obtained with Cr:YAG as saturable absorber [11]. Compared with Cr:YAG, V:YAG is also an excellent saturable absorber which can provide wide absorption band range from 350 to 1600 nm including $^3A_2(^3F) \rightarrow {}^1E(^1D)$ transition for 1.06 μm and $^3A_2(^3F) \rightarrow {}^3T_2(^3F)$ transition for 1.34 μm, which fits the laser emission of the Nd^{3+}-doped crystals well [12]. The advantages of high damage threshold, good thermal conductivity, stable physical properties, and large ground absorption cross sections make V:YAG favorable for efficient dual-wavelength Q-switching operation at 1.06 and 1.34 μm. It was reported that the simultaneous dual-wavelength Q-switching operation at 1.06 and 1.34 μm could be realized with a V:YAG placed in the shared arm of a two laser cavity [13, 14]. But there has rarely been reported on the simultaneously Q-switching operation at 1.06 and 1.34 μm by one saturable absorber in a resonator as far as we know.

This paper is the demonstration of the efficient Q-switched Nd:YVO_4 laser with a V^{3+}:YAG crystal as saturable absorber, which operates at 1064 and 1342 nm. The maximum total average output power is 2.2 W including 1.3 W for 1064 nm and 0.9 W for 1342 nm, corresponding to an optical-optical conversion efficiency of 28.0%. A rate equation model considering the Gaussian spatial dis-

J.-L. Xu · H.-T. Huang · J.-L. He (✉) · J.-F. Yang · B.-T. Zhang · X.-Q. Yang · F.-Q. Liu
State Key Laboratory of Crystal Materials, Institute of Crystal Materials, Shandong University, Ji'nan 250100, China
e-mail: jlhe@sdu.edu.cn

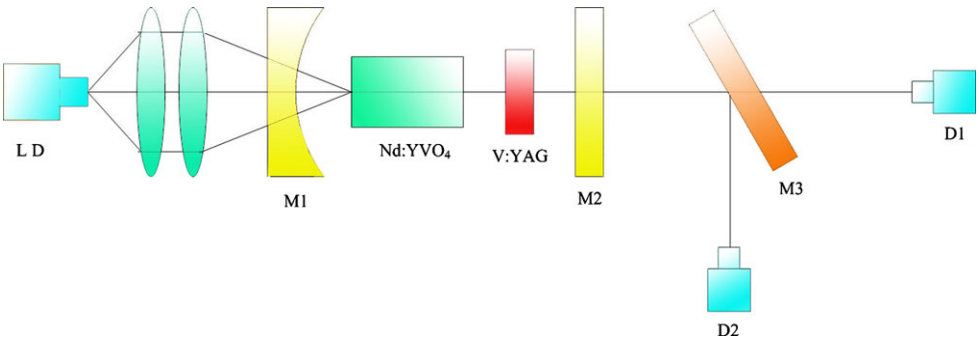

Fig. 1 The schematic of experimental laser setup

tributions of the intracavity photon density and the initial population-inversion density is presented to analyze the performance of the dual-wavelength Q-switching.

2 Experimental setup

The schematic arrangement of the laser setup is shown in Fig. 1. A two-mirror resonator is used to realize dual-wavelength oscillation. A fiber-coupled laser diode array emitting at 808 nm with the core diameter of 400 μm and numerical aperture of 0.22 is used as the pump source. The laser crystal is a $4 \times 4 \times 8$ mm^3 a-cut Nd:YVO_4 with the Nd^{3+} doping level of 0.3 at.%. The two faces are antireflection (AR) coated at 808, 1064 and 1342 nm. It is wrapped by indium foil and mounted in a copper block whose temperature is kept at 21°C by water cooling. A 0.5 mm thick V:YAG with AR coated at 1342 nm is used as the saturable absorber. It is also kept at 21°C to remove the stored heat. Its initial signal transmissions are $T_{01} = 97\%$ at 1064 nm and $T_{02} = 94\%$ at 1342 nm. The input coupler M1 ($R =$ 100 mm) is AR coated at 808 nm on the first side, high reflection (HR) coated at 1064 and 1342 nm on the second side. A plane mirror with the reflectivity of $R_1 = 60\%$ at 1064 nm and $R_2 = 97\%$ at 1342 nm is chosen as the output coupler M2 to realized dual-wavelength Q-switching operation (such a choice will be explained in Sect. 4). The V:YAG is located close to M2. The length of the plano-concave laser cavity is set at 33 mm. A plane mirror M3 with HR coated at 1342 nm and high transmission (HT) coated at 1064 nm is used to separate the output laser. The two beams are detected by the detector D1 and D2 at the same time, and recorded by a digital oscilloscope (1 GHz bandwidth, 5 Gs/s sampling rate).

3 Results and discussions

Firstly, the performance of the continuous wave operation is studied without the V:YAG piece in the cavity. The 1342-nm laser starts oscillating under the incident pump power of

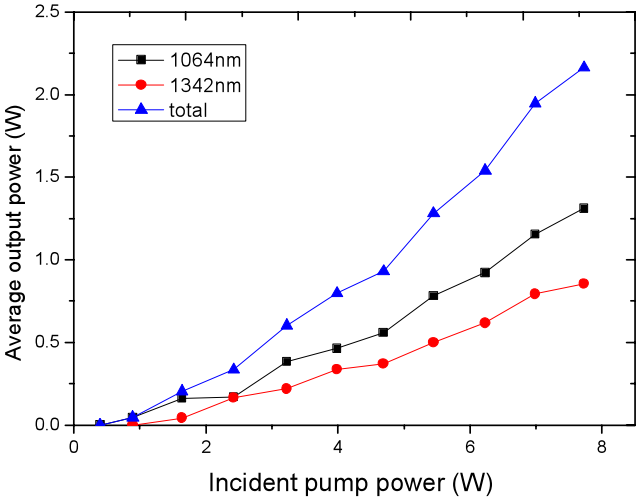

Fig. 2 Average output powers versus the incident pump power for total, 1064 and 1342 nm

0.2 W. But when the incident pump power is increased to 7.7 W, the oscillation at 1064 nm is still not realized. It can be attributed to the losses induced from the high transmission of the output coupler at 1064 nm (13 times larger than that at 1342 nm). When V:YAG is inserted into the laser cavity, the gain balance of the dual wavelengths can be attained. The dual-wavelength passive Q-switching operation is realized under the threshold pump power of 0.4 W for 1064 nm and 0.9 W for 1342 nm. Figure 2 depicts the variation of the 1064-nm, 1342-nm and total average output powers with the pump power. The maximum total average output power is 2.2 W including 1.3 W for 1064 nm and 0.9 W for 1342 nm under the incident pump power of 7.7 W, corresponding to an optical conversion efficiency of 28.2% from the incident pump power to the total average output power. By using of the knife-edge scanning method [15], the quality parameter M^2 factors are, respectively, measured to be around 1.6 and 1.4 for 1064 and 1342 nm.

The dependences of the pulse width and repetition rate on the incident pump power are respectively presented in Figs. 3 and 4. When the incident pump power is lower than 5.5 W the pulse width decreases rapidly with increasing incident pump power. But if the incident pump power is higher

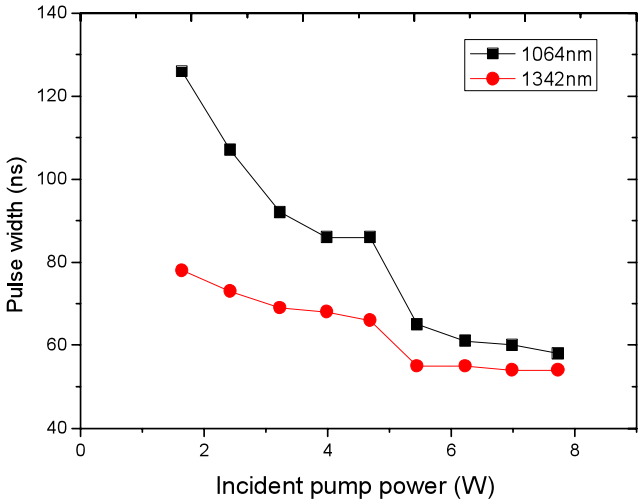

Fig. 3 Pulse width versus the incident pump power for 1064 and 1342 nm

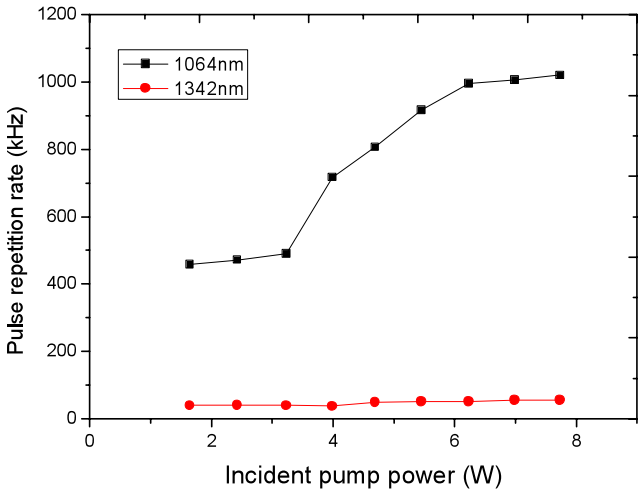

Fig. 4 Pulse repetition rate versus the incident pump power. The trace of 1064 nm refers to the repetition rate between two pulses in a trace cluster

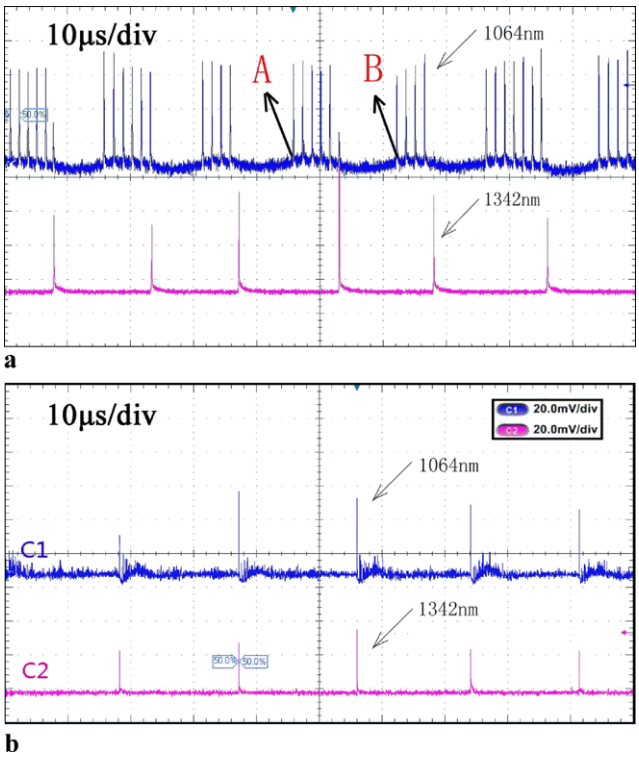

Fig. 5 Pulse trains of 1064 and 1342 nm. (**a**) Under the incident pump power of 1.6 W. (**b**) Under the incident pump power of 7.7 W

than 5.5 W, this trend becomes unnoticeable. It is because the population inversion density is depleted at a very short time and the pulse width is saturated. The pulse widths of 58 and 54 ns are achieved under the incident pump power of 7.7 W for 1064 and 1342 nm, respectively. The repetition rate for the 1064-nm pulses can reach ∼1.0 MHz at the incident pump power of 7.7 W. In the same situation, the repetition rate of 1342 nm is 89 kHz with the peak powers of 180 W.

The interactions between the 1064 and 1342 nm operations are obviously observed on the oscilloscope. The performance under the incident pump power of 1.6 W is taken as an example, and the corresponding pulse trains are shown in Fig. 5a. The time interval between A and B is a total Q-switched period for the two wavelengths. As in Fig. 5a, the 1064-nm traces between two adjacent 1342-nm pulses are in pulse cluster form as that observed in the dual-wavelength passively Q-switched Nd:YVO_4/Cr:YAG/V:YAG laser reported by our group [16]. The repetition rate of the pulse clusters is the same as that of the 1342 nm pulses. According to the conclusion presented in Ref. [17], in the Q-switching situation the ratio of the threshold population-inversion density between 1064 and 1342 nm is less than 1 in our experiment. So the threshold inversion population of 1064-nm laser can be reached earlier than that of 1342 nm under a certain pump rate. It can be clearly seen in Fig. 5a, V:YAG is first bleached by 1064-nm fluorescence in a total Q-switched period.

From close observation on the pulse traces in Fig. 5a, the last pulse in a 1064-nm trace cluster and the 1342-nm single pulse are simultaneously generated at intervals. With increased incident pump power, the simultaneous oscillation trends toward stability. A good performance of the simultaneous oscillation is observed under a pump power of 7.7 W as shown in Fig. 5b. The corresponding expanded waveforms are presented in Fig. 6 with pulse widths of 58 and 54 ns for 1064 and 1342 nm, respectively. The simultaneous generation of the dual-wavelength pulses maybe attributed to very high accumulated inversion population under a relatively high pump power. When the V:YAG is bleached by the 1342-nm fluorescence, such high inversion population will transit to the ground state instantaneously, result-

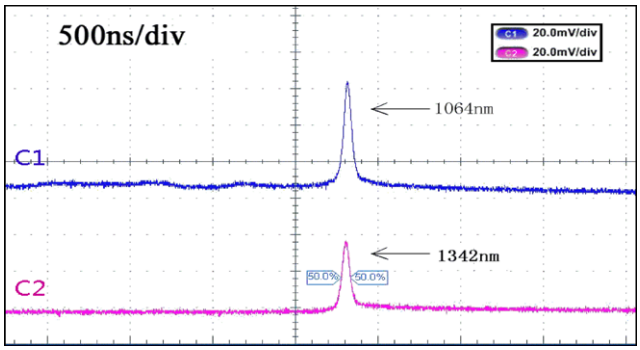

Fig. 6 Single pulse waveform under the incident pump power of 7.7 W

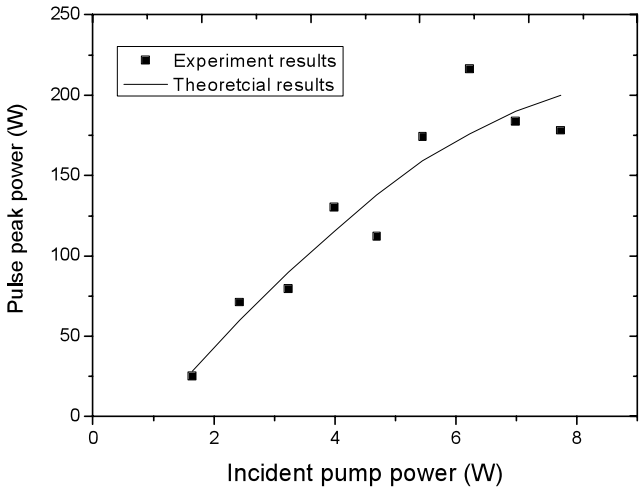

Fig. 7 Pulse peak power for 1342-nm transition versus the incident pump power

ing in the simultaneous building up of a 1064-nm pulse and a 1342-nm pulse. But the simultaneous oscillation is unstable under low incident pump power for the reason that the residual inversion population is not enough to generate a 1064-nm pulse. On close observation of Figs. 5b and 6, the intensity of the 1032-nm pulses is about equal to that of the 1064-nm synchronized pulses. It can be roughly supposed that 0.9 W of the total 1064-nm output power is in the synchronized pulses. Such a device can be fit into a small diode-laser package powered by batteries, which fits the requirement of compact and efficient yellow-orange laser.

According to the average output power, repetition rate and pulse width, the dependence of the pulse peak power for 1342-nm emission on the incident pump power is shown as dots in Fig. 7. One cannot make a precise calculation of the peak power of 1064-nm pulses, since most of the pulses in a trace cluster are of different energy from Fig. 5.

4 The rate equation model

Rate equations are the standard tools for analyzing the performance of the dual-wavelength passively Q-switched laser. The rate equations under plane-wave approximation for the dual-wavelength Q-switched laser are given in Refs. [14, 18]. Recently, it has been shown that the rate equation model established by the assumption that the intracavity photon density and the initial population-inversion density in the rate equations are Gaussian spatial distributions can more accurately simulate the characteristics of the passively Q-switched laser [17, 19].

Supposing the quantum efficiency to be the same for both wavelength and based on Refs. [17–19], the coupled rate equations for the dual-wavelength laser Q-switched by a saturable absorber considering the Gaussian spatial distributions of the intracavity photon density and the initial population-inversion density are described by

$$\begin{aligned}
&\int_0^\infty \frac{\mathrm{d}\phi_i(r,t)}{\mathrm{d}t} 2\pi r\,\mathrm{d}r \\
&= \int_0^\infty \frac{1}{t_r}\Big\{2\sigma_i n(r,t) l \phi_{gi}(r,t) - 2\sigma_{gsi} n_s(r,t) l_s \phi_{gi}(r,t) \\
&\quad - 2\sigma_{esi}\big[n_{s0} - n_s(r,t)\big] l_s \phi_{si}(r,t) \\
&\quad - \delta_{Tgi}\phi_{gi}(r,t) - \delta_{Tsi}\phi_{si}(r,t) \\
&\quad - \ln\left(\frac{1}{R_i}\right)\phi_i(r,t) - L_i\phi_i(r,t)\Big\} 2\pi r\,\mathrm{d}r \\
&\quad (i = 1, 2),
\end{aligned} \tag{1}$$

$$\frac{\mathrm{d}n(r,t)}{\mathrm{d}t} = R_\mathrm{n}(r) - \sigma_1 c n(r,t)\phi_{g1}(r,t) - \sigma_2 c n(r,t)\phi_{g2}(r,t), \tag{2}$$

$$\frac{\mathrm{d}n_s(r,t)}{\mathrm{d}t} = -\sigma_{gs1} c n_s(r,t)\phi_{s1}(r,t) - \sigma_{gs2} c n_s(r,t)\phi_{s2}(r,t) \tag{3}$$

where, $i = 1, 2$ refers to the wavelength 1 and wavelength 2. $\phi(r,t) = \phi(0,t)\exp(-2r^2/\omega_l^2)$ is the average intracavity photon density, where $\phi(0,t)$ is the photon density in the laser axis. $\phi_g(r,t) = (\omega_l^2/\omega_g^2)\phi(0,t)\exp(-2r^2/\omega_g^2)$ is the photon density in the gain medium. $\phi_s(r,t) = (\omega_l^2/\omega_s^2)\phi(0,t)\exp(-2r^2/\omega_s^2)$ is the photon density in the saturable absorber. ω_l is the average radius of the oscillating TEM_{00} mode in the cavity. ω_g and ω_s are the radii of the TEM_{00} mode in the gain medium and saturable absorber, respectively. $t_r = 2l'/c$ is the round-trip time in the cavity with the optical length l'. σ and l are the stimulated emission cross section and length of the gain medium, respectively. σ_{gs} and σ_{es} are ground- and excited-state absorption cross sections of the saturable absorber, respectively. $R_n(r) = \frac{P_{in}[1-\exp(-\alpha l)]}{h\nu_p \pi l \varpi_p^2}$ is the pumping rate, where P_{in}, ϖ_p, α, and

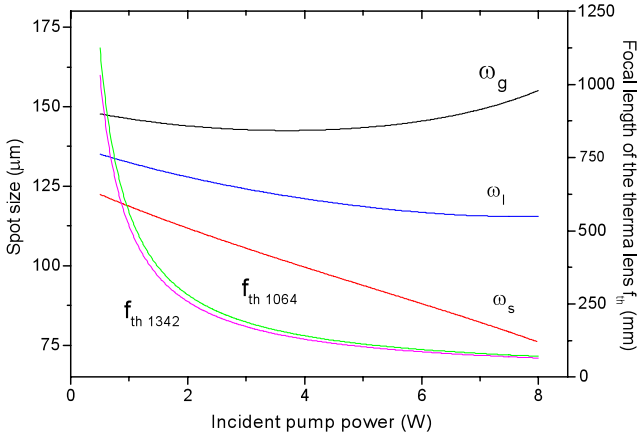

Fig. 8 Focal length of the thermal lens of Nd:YVO_4 and mode size versus the incident pump power

hv_p are the incident pump power, average radius of the pump beam, absorption coefficient of the gain medium, and photon energy of the pump light, respectively. (r, t) is the total instantaneous population-inversion density of the two wavelengths. n_{s0} and $n_s(r, t)$ are, respectively, the total and ground-state population densities of the saturable absorber. l_s is the length of the saturable absorber. δ_{Tg} and δ_{Ts} are the diffraction losses induced by thermal effect in the gain medium and saturable absorber, respectively. R is the reflectivity of the output mirror, and L is the intracavity round-trip dissipative optical loss.

The values of ω_l, ω_g and ω_s depending on the incident pump power are calculated by ABCD matrix theory. The relation between the focal length f_{th} of the thermal lens of the gain medium and the pump power, which is used in the ABCD modeling, can be approximately given by [20]

$$f_{\text{th}} = \frac{4\pi K_c \varpi_p^2}{\zeta P_{in}[\frac{\mathrm{d}n_0}{\mathrm{d}t} + (n_0 - 1)a_T]} \tag{4}$$

where ζ is the fractional thermal loading, K_c is the thermal conductivity, n_0 is the refractive index of the gain medium, $\frac{\mathrm{d}n_0}{\mathrm{d}t}$ is the thermo-optic coefficient of n_0, a_T is the thermal expansion coefficient. The parameters for our experiment are: $n_0 = 2.16$ and 1.96 for 1064 and 1342 nm, respectively; $\zeta \approx 0.25$ and 0.4 for 1064 and 1342 nm, respectively (the nonradiative relaxations from nonradiative sites and concentration quenching are neglected); $K_c = 0.0523$ W/K cm, $\frac{\mathrm{d}n_0}{\mathrm{d}t} = 3.0 \times 10^{-6}$/K, $a_T = 4.43 \times 10^{-6}$/K [21]. According to (4), f_{th} at 1064 nm is close to that at 1342 nm (seeing Fig. 8), thus for simplifying following calculation the f_{th} at both wavelengths are assumed to be equal to unity. Dependences of f_{th} at 1064 nm, ω_l, ω_g and ω_s on the incident pump power are respectively shown in Fig. 8.

The initial conditions of (1)–(3) are

$$\begin{aligned} n(r,0) &= n_1(r,0) + n_2(r,0) \\ &= n_1(0,0)\exp\left(-\frac{2r^2}{\varpi_p^2}\right) + n_2(0,0)\exp\left(-\frac{2r^2}{\varpi_p^2}\right), \end{aligned} \tag{5}$$

$$n_s(r,0) = n_{s0} \tag{6}$$

where $n(r,0)$ is the initial population-inversion density at the position of r. $n(0,0)$ is initial population-inversion density in the laser axis

$$\begin{aligned} &n_1(0,0) \\ &= \frac{[\ln(\frac{1}{R_1}) + \ln(\frac{1}{T_{01}^2}) + \delta_{Tg1} + \delta_{Ts1} + L_1]}{2\sigma_1 l}\left(1 + \frac{\omega_l^2}{\varpi_p^2}\right), \end{aligned} \tag{7}$$

$$\begin{aligned} &n_2(0,0) \\ &= \frac{[\ln(\frac{1}{R_2}) + \ln(\frac{1}{T_{02}^2}) + \delta_{Tg2} + \delta_{Ts2} + L_2]}{2\sigma_2 l}\left(1 + \frac{\omega_l^2}{\varpi_p^2}\right) \end{aligned} \tag{8}$$

where, T_0 is the initial transmission of the saturable absorber.

Substituting (5)–(8) into (2) and (3), the equations are transformed as

$$\begin{aligned} n(r,t) = {} & \exp\left[-\sigma_1 c\left(\frac{\omega_l^2}{\omega_g^2}\right)\exp\left[-\frac{2r^2}{\omega_g^2}\left(\frac{1}{\varpi_p^2} + \frac{1}{\omega_l^2}\right)\right]\right. \\ & \left.\times \int_0^t \phi_1(0,t)\,\mathrm{d}t\right] \\ & \times \left\{R_{\text{in}}\exp\left(-\frac{2r^2}{\varpi_p^2}\right)\int_0^t \exp\left[\sigma_1 c\left(\frac{\omega_l^2}{\omega_g^2}\right)\right.\right. \\ & \left.\times \exp\left(-\frac{2r^2}{\omega_g^2}\right)\int_0^t \phi_1(0,t)\,\mathrm{d}t\right]\mathrm{d}t \\ & \left.+ n_1(0,0)\exp\left(-\frac{2r^2}{\varpi_p^2}\right)\right\} + \exp\left[-\sigma_2 c\left(\frac{\omega_l^2}{\omega_g^2}\right)\right. \\ & \left.\times \exp\left(-\frac{2r^2}{\omega_g^2}\right)\int_0^t \phi_2(0,t)\,\mathrm{d}t\right] \\ & \times \left\{R_{\text{in}}\exp\left(-\frac{2r^2}{\varpi_p^2}\right)\int_0^t \exp\left[\sigma_2 c\left(\frac{\omega_l^2}{\omega_g^2}\right)\right.\right. \\ & \left.\times \exp\left(-\frac{2r^2}{\omega_g^2}\right)\int_0^t \phi_2(0,t)\,\mathrm{d}t\right]\mathrm{d}t \\ & \left.+ n_2(0,0)\exp\left(-\frac{2r^2}{\varpi_p^2}\right)\right\}, \end{aligned} \tag{9}$$

$$\begin{aligned} &n_s(r,t) \\ &= n_{s0}\left\{\exp\left[-\sigma_{gs1} c\left(\frac{\omega_l^2}{\omega_s^2}\right)\exp\left(-\frac{2r^2}{\omega_s^2}\right)\int_0^t \phi_1(0,t)\,\mathrm{d}t\right]\right. \end{aligned}$$

$$+\exp\left[-\sigma_{gs2}c\left(\frac{\omega_l^2}{\omega_s^2}\right)\exp\left(-\frac{2r^2}{\omega_s^2}\right)\int_0^t \phi_2(0,t)\,\mathrm{d}t\right]\Bigg\}. \tag{10}$$

Substituting (9) and (10) into (1), then we can obtain

$$\begin{aligned}\frac{\mathrm{d}\phi_i(0,t)}{\mathrm{d}t} = \frac{4\phi_i(0,t)}{\omega_l^2 t_r}\int_0^\infty \Bigg\{ & 2\sigma_i n(r,t) l\left(\frac{\omega_l^4}{\omega_g^2}\right) \\ & \times \exp\left[-\frac{2r^2}{\omega_g^2}\left(\frac{1}{\varpi_p^2}+\frac{1}{\omega_l^2}\right)\right] \\ & - 2\sigma_{gsi} n_s(r,t) l_s\left(\frac{\omega_l^2}{\omega_s^2}\right)\exp\left(-\frac{2r^2}{\omega_s^2}\right) \\ & - 2\sigma_{esi}\left[n_{s0}-n_s(r,t)\right] l_s\left(\frac{\omega_l^2}{\omega_s^2}\right)\exp\left(-\frac{2r^2}{\omega_s^2}\right) \\ & - \delta_{Tgi}\left(\frac{\omega_l^2}{\omega_g^2}\right)\exp\left(-\frac{2r^2}{\omega_g^2}\right) \\ & - \delta_{Tsi}\left(\frac{\omega_l^2}{\omega_s^2}\right)\exp\left(-\frac{2r^2}{\omega_s^2}\right) \\ & - \ln\left(\frac{1}{R_i}\right)\exp\left(-\frac{2r^2}{\omega_l^2}\right) \\ & - L_i\exp\left(-\frac{2r^2}{\omega_l^2}\right)\Bigg\} r\,\mathrm{d}r \end{aligned}$$

$$(i=1,2). \tag{11}$$

Equation (11) can be solved numerically for the dual-wavelength passively Q-switched laser operated at 1064 and 1342 nm, with V:YAG as saturable absorber under the incident pump power of 7.7 W. The parameters used in the calculation are: $i = 1, 2$ refers to 1064 and 1342 nm, respectively; $\varpi_p = 200$ μm, $\omega_g = 153$ μm, $\omega_s = 78$ μm, $\omega_l = 115$ μm, $l = 8$ mm, $l_s = 0.5$ mm, $R_1 = 60\%$, $R_2 = 97\%$, $\sigma_1 = 2.5 \times 10^{-18}$ cm^2, $\sigma_2 = 0.76 \times 10^{-18}$ cm^2, $\sigma_{gs1} = 3.1 \times 10^{-18}$ cm^2, $\sigma_{gs2} = 7.2 \times 10^{-18}$ cm^2, $\sigma_{es1} = 1.4 \times 10^{-19}$ cm^2, and $\sigma_{es2} = 7.4 \times 10^{-19}$ cm^2 [5]. The yields of (11) at the incident pump power of 7.7 W are shown in Figs. 9a and b, which represent the interaction effect between 1064 and 1342 nm laser well. Compared with Fig. 5b, the theoretical simulation is in agreement with our experimental phenomena.

According to the method of Ref. [22] the expressions for single pulse peak power P and energy E can be obtained as

$$P_i = \frac{\pi h v_i \omega_s^2}{4\sigma_i t_r}\ln\left(\frac{1}{R_i}\right)\phi_{sm_i} \quad (i=1,2), \tag{12}$$

$$E_i = \frac{\pi h v_i \omega_s^2}{4\sigma_i t_r}\ln\left(\frac{1}{R_i}\right)\phi_{\mathrm{integ}_i} \quad (i=1,2) \tag{13}$$

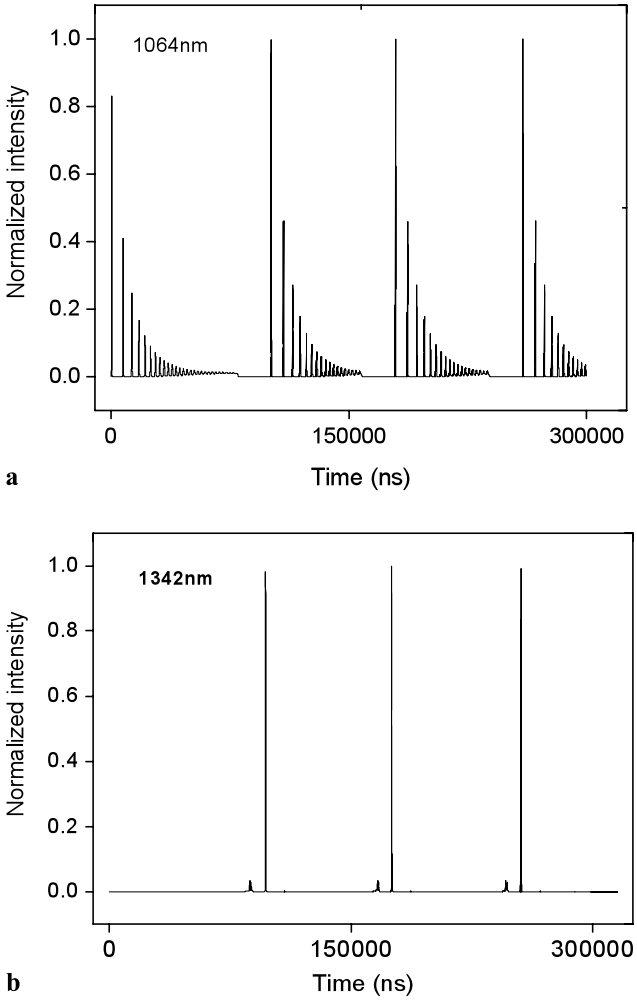

Fig. 9 Calculated pulse trains under the incident pump power of 7.7 W

where ϕ_{sm_i} is the maximum value of $\phi(0,t)$, and ϕ_{integ} is the integral of $\phi(0,t)$ over t from zero to infinity. Using (13) and the above parameters, the theoretical dependence of the single-pulse peak power for 1342-nm transition on the incident pump power can be calculated and is shown in Fig. 7.

To optimize a simultaneously dual-wavelength passively Q-switched laser if we have a saturable absorber with defined initial transmission, it is essential to choose the reflectivity values of the output couplers to balance the gain for both output wavelengths. The choice bases on two considerations—same threshold or same pulse peak power. The Q-switched operation will begin when the population-inversion density crosses the initial threshold value. Since $T_0 = \exp(-\sigma_{gs} n_{s0} l_s)$ and $n_s(0,0) = n_{s0}$, the initial population-inversion density can be obtained as follows when setting (10) to zero and $t = 0$

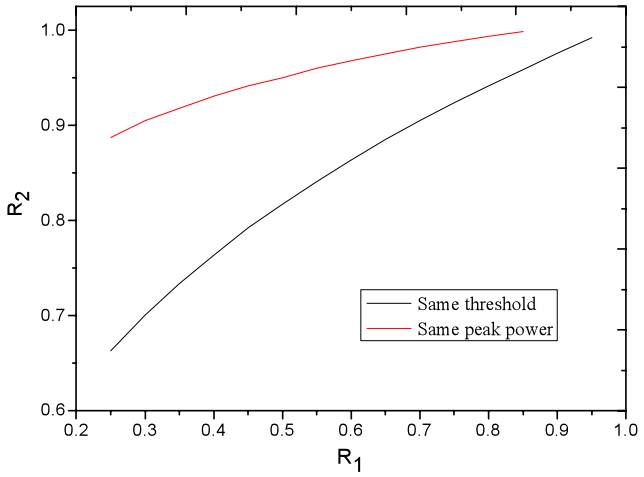

Fig. 10 Output coupler reflectivity R_2 at 1342 nm as a function of R_1 at 1064 nm for conditions of same lasing threshold or same pulse peak power

$$n_i(0,0) = \frac{\ln(\frac{1}{R_i}) + \ln(\frac{1}{T_{0i}^2}) + \delta_{Tgi} + \delta_{Tsi} + L_i}{2\sigma_i l}\left(1 + \frac{\omega_l^2}{\varpi_p^2}\right) \quad (i = 1, 2). \tag{14}$$

From (14), in order to let the threshold is the same for both transitions, i.e. $n_1(0,0) = n_2(0,0)$, the appropriate relation between the two output coupler transmissions can be given by

$$R_2 = \exp\left\{\sigma_1\left[\ln\left(\frac{1}{T_{02}^2}\right) + \delta_{Tg2} + \delta_{Ts2} + L_2\right]\sigma_1^{-1} - \sigma_2\left[\ln\left(\frac{1}{R_1}\right) + \ln\left(\frac{1}{T_{01}^2}\right) + \delta_{Tg1} + \delta_{Ts1} + L_1\right]\sigma_1^{-1}\right\}. \tag{15}$$

With the above parameters, the corresponding variation of R_2 with R_1 is shown in Fig. 10. It can be seen that R_2 almost increases linearly with R_1.

In many practical applications (for example, in frequency mixing), it is more crucial to use special coatings for both wavelengths to achieve same peak power of the synchronized pulses. In such condition, according to (12), the relationship between R_1 and R_2 will be

$$R_2 = \exp\left[-\frac{\sigma_2 v_1 \ln(\frac{1}{R_1})\phi_{sm1}}{\sigma_1 v_2 \phi_{sm2}}\right] \tag{16}$$

By solving (11) and (16), the relationship between R_1 and R_2 when P_1 and P_2 reach the same value under the incident pump power of 7.7 W is shown in Fig. 10. When R_1 is defined, the value of R_2 is significant larger than that in the condition that both transitions possess the same threshold. If R_1 is assumed to be 0.6, R_2 is calculated to be ~0.97 to satisfy same peak power, which fits the output coupler transmission we designed in the experiment.

5 Conclusion

The simultaneously dual-wavelength passively Q-switched laser at 1064 and 1342 nm with a V:YAG saturable absorber in a plano-concave cavity is demonstrated. The maximum dual-wavelength average output power of 2.2 W is obtained with 1.3 W for 1064 nm and 0.9 W for 1342 nm, corresponding to a total optical-optical conversion efficiency of 28.2%. Moreover, we describe a rate equation model of the passively dual-wavelength Q-switched laser considering the spatial Gaussian distribution of intracavity photon density. The theoretical simulation is in agreement with our experimental phenomena. Simple rules for designing such a laser are also derived. We believe that this simultaneous dual-wavelength laser can be applied in compact, low-cost, efficient yellow-orange laser in the future.

Acknowledgements This work was supported by the National Natural Science Foundation of China (Grant No: 60878012, and 50721002), and Program for Taishan Scholars. He Jing-Liang's e-mail address is jlhe@sdu.edu.cn.

References

1. P.X. Li, D.H. Li, C.Y. Li, Z.G. Zhang, Opt. Commun. **235**, 169 (2004)
2. Y. Lu, B.G. Zhang, E.B. Li, D.G. Xu, R. Zhou, X. Zhao, F. Ji, T.L. Zhang, P. Wang, J.Q. Yao, Opt. Commun. **262**, 241 (2006)
3. K. Lünstedt, N. Pavel, K. Petermann, G. Huber, Appl. Phys. B **86**, 65 (2007)
4. Y.F. Chen, Appl. Phys. B **70**, 475 (2000)
5. J.L. He, J. Du, J. Sun, S. Liu, Y.X. Fan, H.T. Wang, L.H. Zhang, Y. Hang, Appl. Phys. B **79**, 301 (2004)
6. Y. E Hou, Y.X. Fan, J.L. He, H.T. Wang, Opt. Commun. **265**, 301 (2006)
7. K. Spariosu, W. Chen, R. Stultz, M. Birnbaum, A.V. Shestakov, Opt. Lett. **18**, 814 (1993)
8. A.V. Podlipensky, K.V. Yumashev et al., Appl. Phys. B **76**, 245 (2003)
9. F.Q. Liu, J.L. He, B.T. Zhang, J.L. Xu, X.L. Dong, K.J. Yang, H.R. Xia, H.J. Zhang, Opt. Express **16**, 11759 (2008)
10. I.A. Denisov, M.I. Demchuk, N.V. Kuleshov, K.V. Yumashev, Appl. Phys. Lett. **77**, 2455 (2000)
11. L. Zhang, Z.Y. Wei, B.H. Feng, D.H. Li, Z.G. Zhang, Opt. Commun. **264**, 51 (2006)
12. A.M. Malyarevich, I.A. Denisov, K.V. Yumashev, V.P. Mikhailov, R.S. Conroy, B.D. Sinclair, Appl. Phys. B **67**, 555 (1998)
13. P. Tidemand-Lichtenberg, J. Janousek, R. Melich, J.L. Mortensen, P. Buchhave, Opt. Commun. **241**, 487 (2004)
14. J. Janousek, P. Tidemand-Lichtenberg, J.L. Mortensen, P. Buchhave, Opt. Commun. **265**, 277 (2006)
15. H.R. Bilger, T. Habib, Appl. Opt. **24**, 686 (1985)
16. H.T. Huang, J.L. He, B.T. Zhang, K.J. Yang, C.H. Zuo, J.L. Xu, X.L. Dong, S. Zhao, Appl. Phys. B **96**, 815 (2009)

17. X. Zhang, S. Zhao, Q. Wang, B. Ozygus, H. Weber, J. Opt. Soc. Am. B **17**, 1166 (2000)
18. George A. Henderson, J. Appl. Phys. **68**, 5451 (1990)
19. G.Q. Li, S.Z. Zhao, H.M. Zhao, K.J. Yang, S.H. Ding, Opt. Commun. **234**, 321 (2004)
20. S.C. Tidwell, J.F. Seamans, M.S. Bowers, A.K. Cousins, IEEE J. Quantum Electron. **28**, 997 (1992)
21. Y.F. Chen, S.W. Tsai, Opt. Lett. **397**, 27 (2002)
22. J.J. Degnan, IEEE J. Quantum Electron. **25**, 214 (1989)